Eurographics Symposium on Geometry Processing (2004)
R. Scopigno, D. Zorin (Editors)

Second Order Smoothness over Extraordinary Vertices

Charles Loop

Microsoft Research

Abstract

Catmull & Clark subdivision is now a standard for smooth free-form surface modeling. These surfaces are everywhere curvature continuous except at points corresponding to vertices not incident on four edges. While the surface has a continuous tangent plane at such a point, the lack of curvature continuity presents a severe problem for many applications. Topologically, each n-valent extraordinary vertex of a Catmull & Clark limit surface corresponds to an n-sided hole in the underlying 2-manifold represented by the control mesh. The problem we address here is: How to fill such a hole in a Catmull & Clark surface with exactly n tensor product patches that meet the surrounding bicubic patch network and each other with second order continuity. We convert the problem of filling the hole with n tensor product patches in the spatial domain into the problem of filling the hole in the n frequency modes with a single bidegree 7 tensor product patch.

Categories and Subject Descriptors (according to ACM CCS): I.3.5 [Computer Graphics]: Curve, surface, solid, and object representations

1. Introduction

Subdivision techniques for modeling smooth free-form surfaces have become popular in recent years due largely to their ability to represent surfaces of arbitrary topological type. The surfaces of Catmull & Clark [CC78] have supplanted NURBS in many graphics applications [DKT98]. However, these techniques have not seen wide acceptance in the CAD and engineering world due to the lack of second order continuity at so-called *extraordinary vertices* - vertices not incident on four edges. Catmull & Clark surfaces are everywhere C^2 except at finite collection of such points. This defect is a severe limitation for applications that require *class A* surfaces.

A Catmull & Clark surface is a smooth approximation to a 2-manifold control mesh. The subdivision operator iteratively refines and smoothes the control mesh resulting in a limit surface. Refinement preserves topology, meaning the topology of the limit surface is identical to that of the control mesh minus a singularity corresponding to each extraordinary vertex. Each singularity corresponds to a hole in the 2-manifold represented by the control mesh. Such a hole has a circular boundary that we model, up to second order behavior, with a 2-ring of control points about an extraordinary vertex. The cyclic nature of an extraordinary vertex 2-ring suggests a transformation from the spatial domain of control points to a corresponding frequency domain using Fourier methods. This has been used to great affect in the analysis of subdivision surfaces [DS78, Rei95]. We use this transformation to convert the problem of smoothly filling an n-sided hole with n tensor product patches, into n instances of the problem of smoothly filling each spectral band, or *mode* with a single tensor product patch. These *mode patches* are transformed back to the spatial domain resulting in a curvature continuous surface.

Several previous curvature continuous surface schemes have been developed. In [GH89], (non-polynomial) patches are constructed that meet with curvature continuity to fill an n-sided hole in a tensor product patch network. In [Pet96], n degree 8 triangular patches are used to fill an n-sided hole in a generalized four direction box spline surface. Prautzsch [Pra97] proposed a G^2 scheme for hole filling in a quad mesh using bidegree 6 tensor product patches. This approach re-

quires at least three subdivision steps to ensure proper extraordinary vertex separation, and data on perimeter of the hole is modified. Similarly, the construction of [GZ99] consists of biquintic tensor product surfaces, but also modifies the hole and requires $4n$ patches to fill it. Prautzsch and Umlauf [PU00] construct a curvature continuous surface from a triangular mesh after one level of subdivision. Their surface is composed of degree 8 Bézier triangles; requiring $4n$ to fill each hole in a generalized triangular box spline surface. In [Pet02], an n-sided hole is filled with a combination of bicubic and degree 5×3 tensor product surface patches. This approach does not extend to high valence [Pet03], and the low degree again comes at a cost of a high patch count.

Our approach differs from others in that we address the following specific problem: How to fill each n-sided hole, corresponding to an extraordinary vertex in a Catmull & Clark surface, with exactly n tensor product patches that meet the surrounding bicubic tensor product patch network and each other with second order continuity.

This paper is organized as follows. In Section 2 we review background material and discuss some details of our notation. We consider the problem in the frequency domain in Section 3. We construct boundary data in Bézier form in Section 4, followed by a derivation of the constraints needed for a pair of surfaces to meet with second order contact in Section 5. Our construction is presented in Sections 6 through 9, and we gives results in Section 10. We discuss various aspects of this and future work in Section 11, and we finish with conclusions in Section 12.

2. Background

Readers not familiar with Bézier and B-spline curves and surfaces, and the basics of subdivision surfaces are encouraged to consult a good text such as [Far01].

We write a degree d Bézier curve as the product

$$w(t) = \mathbf{B}^d(t)\,\mathbf{w},$$

where $\mathbf{w}$ is a set of *control points* that govern the shape of the curve, and $\mathbf{B}^d(t)$ are the Bernstein polynomials defined

$$\mathbf{B}_i^d(t) = \tbinom{d}{i}(1-t)^{d-i}t^d,$$

with $i = 0,\ldots,d$. We write a degree $r \times s$ Bézier *tensor product* surface

$$w(u,v) = \mathbf{B}^r(u)\,\mathbf{w}\,(\mathbf{B}^s(v))^T,$$

where $\mathbf{w}$ is an $r \times s$ array of points referred to as the *control net*.

We make extensive use of the Discrete Fourier Transform pair, DFT and IDFT[BH95]. Given a set of n points $\mathbf{a}^k \in \mathbb{R}^m$, $k \in \mathbb{Z}_{\bmod n}$, we define

$$\hat{\mathbf{a}} = \mathrm{DFT}(\mathbf{a}), \quad \text{and} \quad \mathbf{a} = \mathrm{IDFT}(\hat{\mathbf{a}}),$$

to be

$$\hat{\mathbf{a}}^l = \tfrac{1}{n}\sum_{k=0}^{n-1} \bar{E}_n^{kl}\mathbf{a}^k, \quad \text{and} \quad \mathbf{a}^k = \sum_{l=0}^{n-1} E_n^{kl}\hat{\mathbf{a}}^l,$$

where $k,l = 0,\ldots,n-1$,

$$E_n^i = C_n^i + \mathbb{I}S_n^i, \quad \text{and} \quad \bar{E}_n^i = C_n^i - \mathbb{I}S_n^i$$

are the Euler relations with

$$C_n^i = \cos\frac{2\pi i}{n}, \quad S_n^i = \sin\frac{2\pi i}{n}, \quad \text{and} \quad \mathbb{I} = \sqrt{-1}.$$

Note that we drop the superscripts when $i = 1$. The DFT transforms points in the spatial domain to spectral bands, or frequency *modes*. Its inverse, the IDFT transforms frequency modes to spatial domain points. The spatial domain consists of points in $\mathbb{R}^m$, while the frequency domain consists of points in $\mathbb{C}^m$. Readers not familiar with the special properties of complex numbers can find an excellent overview in [Nee97].

We make general use of the concept of a d-ring about an extraordinary vertex. We define a d-ring $\mathbf{p}$ to be a rank 3 tensor consisting of n overlapping $(d+1)\times(d+1)$ arrays of points. We refer to a single point belonging to a d-ring as $\mathbf{p}_{ij}^l$, where $l \in \mathbb{Z}_{\bmod n}$ refers to an array and i and j are array indices (since these are never double digits here we ignore a ',' separator). The n arrays pairwise share points along an edge

$$\mathbf{p}_{i0}^l = \mathbf{p}_{0i}^{l+1} \quad i = 0,\ldots,d,$$

and all arrays share the point

$$\mathbf{p}_{00}^0 = \mathbf{p}_{00}^1 = \cdots = \mathbf{p}_{00}^{n-1}.$$

3. Problem Transformation

We begin our construction with a 2-ring of control points $\mathbf{a}$ that enclose a valence n extraordinary vertex represented by $\mathbf{a}_{00}$, see Figure 1. This configuration of points might be the result of two or more steps of Catmull & Clark subdivision, or they could be specified arbitrarily. Our goal is to construct n tensor product patches, corresponding to the n arrays of the 2-ring, that meet with second order continuity along adjacent boundaries, and with the implied bicubic tensor product patch network that surrounds the extraordinary vertex.

More formally, we seek a surface $\mathcal{A}\colon \Omega_k \to \mathbb{R}^m$, $k \in \mathbb{Z}_{\bmod n}$, where each Ω_k is a unit square domain with parameters $u,v \in [0,1]\times[0,1]$. We write $\mathcal{A}$ as a linear combination

$$\mathcal{A}(k,u,v) = \mathbf{A}(k,u,v)\,\mathbf{a}, \tag{1}$$

where $\mathbf{A}$ is a collection of basis functions and $\mathbf{a}$ is a 2-ring of control points.

We will construct this surface so that edges $u = 1$ and $v = 1$ correspond to the perimeter of the extraordinary vertex hole; we refer to these as *external* edges. The edges

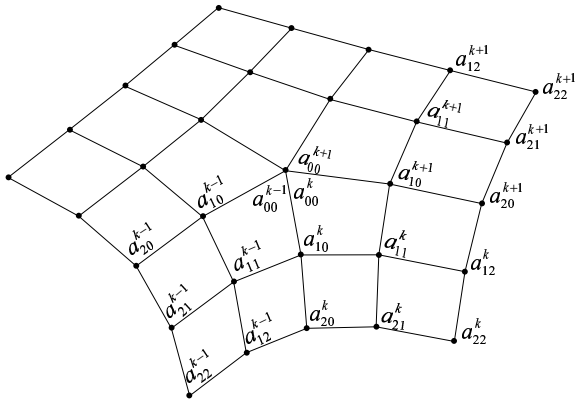

Figure 1: *A 2-ring **a** with point labeling.*

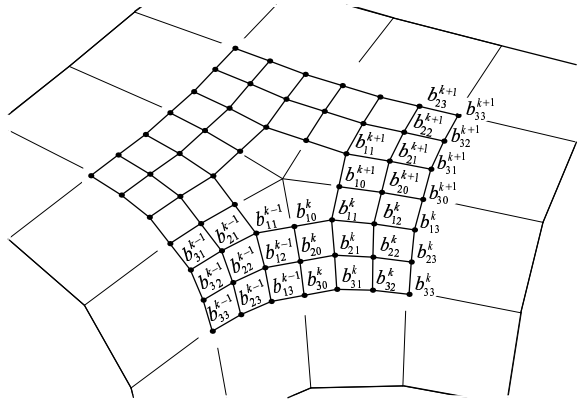

Figure 2: *The n bicubic Bézier nets that characterize second order behavior on the boundary of an extraordinary vertex hole.*

where $u = 0$ and $v = 0$ will correspond to the shared edges $\mathcal{A}(k,u,0) = \mathcal{A}(k+1,0,v)$; we refer to these as *internal* edges.

We will formulate constraints for second order contact on the internal edges in Section 5. If we solve for the smoothness constraints in the spatial domain, we need to solve an $O(n)$ system of equations. By transforming the problem into the frequency domain we instead solve n $O(1)$ systems. We make use of the Discrete Fourier Transform (DFT) and find the related surface

$$\hat{\mathcal{A}}(l,u,v) = \hat{\mathbf{A}}(l,u,v)\,\hat{\mathbf{a}}$$

where

$$\hat{\mathbf{a}} = \mathrm{DFT}(\mathbf{a}),$$

and $\hat{\mathbf{A}}$ are transformed basis functions. We transform $\hat{\mathcal{A}}(l,u,v)$ back to the spatial domain to get $\mathcal{A}(k,u,v)$.

Next, we consider the constraints imposed by the surrounding tensor product network in both the spatial and frequency domains.

4. Boundary in Bézier Form

We characterize up to second order, the behavior of the tensor product patch network on the boundary of the hole that surrounds an extraordinary vertex. We can think of the surrounding tensor product patch network as n adjacent rectangular B-spline surfaces that are each missing a single patch because the rectangular control point structure needed to define B-splines breaks down at the extraordinary vertex. However, enough of the rectangular structure remains to construct 15 out of 16 of the Bézier control points of each missing bicubic patch. These 15 points completely characterize the second order behavior of the external boundary, see Figure 2.

We find the control points of these bicubic Bézier patches by applying a linear operator on our 2-ring control points to convert from the B-spline basis

$$\mathbf{b}^k = \mathbf{Q}\left[\begin{array}{c|ccc} \cdot & \mathbf{a}_{10}^{k+2} & \mathbf{a}_{11}^{k+1} & \mathbf{a}_{12}^{k+1} \\ \hline \mathbf{a}_{10}^{k-1} & \mathbf{a}_{00}^{k} & \mathbf{a}_{10}^{k+1} & \mathbf{a}_{20}^{k+1} \\ \mathbf{a}_{11}^{k-1} & \mathbf{a}_{10}^{k} & \mathbf{a}_{11}^{k} & \mathbf{a}_{12}^{k} \\ \mathbf{a}_{12}^{k-1} & \mathbf{a}_{20}^{k} & \mathbf{a}_{21}^{k} & \mathbf{a}_{22}^{k} \end{array}\right]\mathbf{Q}^T,$$

where

$$\mathbf{Q} = \frac{1}{6}\begin{bmatrix} 1 & 4 & 1 & 0 \\ 0 & 4 & 2 & 0 \\ 0 & 2 & 4 & 0 \\ 0 & 1 & 4 & 1 \end{bmatrix},$$

and $\mathbf{b}^k$ are arrays of a 3-ring $\mathbf{b}$. The $\cdot$ represents a point that does not affect second order boundary behavior.

Since we are primarily interested in these Bézier nets in the frequency domain, we find $\hat{\mathbf{a}} = \mathrm{DFT}(\mathbf{a})$ to get complex valued points $\hat{\mathbf{b}}$ as

$$\hat{\mathbf{b}}^l = \mathbf{Q}\left[\begin{array}{c|ccc} \cdot & E_n^{2l}\hat{\mathbf{a}}_{10}^l & E_n^l\hat{\mathbf{a}}_{11}^l & E_n^l\hat{\mathbf{a}}_{21}^l \\ \hline \bar{E}_n^l\hat{\mathbf{a}}_{10}^l & \hat{\mathbf{a}}_{00}^l & E_n^l\hat{\mathbf{a}}_{10}^l & E_n^l\hat{\mathbf{a}}_{20}^l \\ \bar{E}_n^l\hat{\mathbf{a}}_{11}^l & \hat{\mathbf{a}}_{10}^l & \hat{\mathbf{a}}_{11}^l & \hat{\mathbf{a}}_{12}^l \\ \bar{E}_n^l\hat{\mathbf{a}}_{12}^l & \hat{\mathbf{a}}_{20}^l & \hat{\mathbf{a}}_{21}^l & \hat{\mathbf{a}}_{22}^l \end{array}\right]\mathbf{Q}^T, \qquad (2)$$

where $l = 0,\cdots,n-1$. We then form complex valued patches

$$\hat{\mathcal{B}}(l,u,v) = \mathbf{B}^3(u)\begin{bmatrix} \cdot & E_n^l\hat{\mathbf{b}}_{10}^l & E_n^l\hat{\mathbf{b}}_{20}^l & E_n^l\hat{\mathbf{b}}_{30}^l \\ \hat{\mathbf{b}}_{10}^l & \hat{\mathbf{b}}_{11}^l & \hat{\mathbf{b}}_{12}^l & \hat{\mathbf{b}}_{13}^l \\ \hat{\mathbf{b}}_{20}^l & \hat{\mathbf{b}}_{21}^l & \hat{\mathbf{b}}_{22}^l & \hat{\mathbf{b}}_{23}^l \\ \hat{\mathbf{b}}_{30}^l & \hat{\mathbf{b}}_{31}^l & \hat{\mathbf{b}}_{32}^l & \hat{\mathbf{b}}_{33}^l \end{bmatrix}\left(\mathbf{B}^3(v)\right)^T.$$

These patches are C^2 with the surrounding tensor product patch network, but in general are only C^0 with each other. These patches are close to the surface that we will ultimately construct; for many applications, they can serve as a lower cost *proxy* geometry for the final surface. The missing control points correspond to $\mathbf{b}_{00}^k$ (similarly $\hat{\mathbf{b}}_{00}^l$). Specifying a

position for $\mathbf{b}_{00}^k$ is not necessary for our construction, but for proxy purposes it should agree with $\mathcal{A}(k,0,0)$

The surface $\hat{\mathcal{B}}(l,u,v)$ (similarly $\mathcal{B}(k,u,v)$) completely characterizes second order behavior on the external boundary. Next, we consider the constraints needed for second order contact.

5. Second Order Contact

We now derive constraints on a pair of surface patches necessary for second order contact. We must consider a more general characterization than strict derivative continuity since, in general, we will not have a global parameterization where derivatives can be taken. We follow the notion put forth in [DeR85] where a parameterization independent form of smoothness is defined. The idea is that two surfaces meet smoothly if one can be reparameterized, via a composition, so that their derivatives agree.

In the following, we avoid the use of more cumbersome differential symbols by placing derivative directions on a function as a superscript sequence; subscripts are used to distinguish vector components.

Definition 1 If $\mathcal{F}$ and $\mathcal{G}$ are maps from $\mathbb{R}^2 \to \mathbb{R}^m$, then $\mathcal{F}$ and $\mathcal{G}$ are said to meet with k^{th} order contact, also called k^{th} order *geometric continuity* denoted G^k, if there exists a map ϕ from $\mathbb{R}^2 \to \mathbb{R}^2$ such that

$$(\mathcal{F}\circ\phi)^{\overbrace{v\cdots v}^{j}}(u,0) = \mathcal{G}^{\overbrace{v\cdots v}^{j}}(u,0) \quad j=0,\ldots,k.$$

Note that (u,v) are parameters in the domain of ϕ and $\mathcal{G}$, and (x,y) will be used for parameters in the domain of $\mathcal{F}$.

We consider the symmetric case where r is a reflection about the x axis and

$$\mathcal{G}(u,0) = (\mathcal{F}\circ\phi)(u,0), \tag{3}$$
$$\mathcal{H}(u,0) = (\mathcal{F}\circ r\circ\phi)(u,0), \tag{4}$$

see Figure 3. Our goal here is to find relations between the derivatives of $\mathcal{G}$ and $\mathcal{H}$ that are needed for second order contact. Assume Definition 1 holds for Equations (3) and (4) when $k=0,1,2$. Since $\mathcal{G}$ and $\mathcal{H}$ share a common boundary curve, we drop $(u,0)$, and $(\phi_x(u,0),0)$ to simplify our notation, and we note that $\mathcal{G}^u = \mathcal{H}^u$, $\mathcal{G}^{uu} = \mathcal{H}^{uu}$, and $\phi_y = \phi_y^u = \phi_y^{uu} = 0$ along the edge $u=0$. Using the chain rule, we have

$$G = F\cdot\Phi \quad \text{and} \quad H = F\cdot R\cdot\Phi,$$

where

$$F = [\mathcal{F}^x, \mathcal{F}^y, \mathcal{F}^{xx}, \mathcal{F}^{xy}, \mathcal{F}^{yy}]^T,$$
$$G = [\mathcal{G}^u, \mathcal{G}^v, \mathcal{G}^{uu}, \mathcal{G}^{uv}, \mathcal{G}^{vv}]^T,$$
$$H = [\mathcal{H}^u, \mathcal{H}^v, \mathcal{H}^{uu}, \mathcal{H}^{uv}, \mathcal{H}^{vv}]^T,$$

and

$$\Phi = \begin{bmatrix} \phi_x^u & \phi_x^v & \phi_x^{uu} & \phi_x^{uv} & \phi_x^{vv} \\ 0 & \phi_y^v & 0 & \phi_y^{uv} & \phi_y^{vv} \\ 0 & 0 & (\phi_x^u)^2 & \phi_x^u\phi_x^v & (\phi_x^v)^2 \\ 0 & 0 & 0 & \phi_x^u\phi_y^v & 2\phi_x^v\phi_y^v \\ 0 & 0 & 0 & 0 & (\phi_y^v)^2 \end{bmatrix},$$

and

$$R = \begin{bmatrix} 1 & 0 & 0 & 0 & 0 \\ 0 & -1 & 0 & 0 & 0 \\ 0 & 0 & 1 & 0 & 0 \\ 0 & 0 & 0 & -1 & 0 \\ 0 & 0 & 0 & 0 & 1 \end{bmatrix}.$$

From this we have two representations for F, namely

$$F = G\cdot\Phi^{-1} \quad \text{and} \quad F = H\cdot(R\cdot\Phi)^{-1}.$$

Equating these and extracting the components corresponding to $\mathcal{F}^y$ and $\mathcal{F}^{yy}$, we arrive at the symmetric G^1 and G^2 constraints

$$2\phi_x^v\mathcal{G}^u = \phi_x^u\left(\mathcal{G}^v + \mathcal{H}^v\right), \tag{$\mathbf{G}^1$}$$

$$2\phi_x^v\phi_y^v\left(\mathcal{G}^{uv} - \mathcal{H}^{uv}\right) = \left(2\phi_x^v\phi_y^{uv} - \phi_x^u\phi_y^{vv}\right)\left(\mathcal{G}^v - \mathcal{H}^v\right) + \phi_x^u\phi_y^v\left(\mathcal{G}^{vv} - \mathcal{H}^{vv}\right) \tag{$\mathbf{G}^2$}$$

6. Our Solution

We use the ideas of Section 5 in two distinct ways to build a G^2 surface. We will construct a cyclically ordered set of tensor product surface patches that satisfy constraints of the form $\mathbf{G}^1$ and $\mathbf{G}^2$ along their shared internal boundaries $u=0$ and $v=0$, with a suitable chosen ϕ. This surface will also maintain second order contact with the boundary surface $\mathcal{B}$ along the external boundaries $u=1$ and $v=1$. The later goal will be accomplished by a reparameterization of the form $\mathcal{B}\circ\psi$ evaluated on $u=1$ and $v=1$. We discuss the derivation of ψ in Section 8.

In order to keep the degree of our G^2 surface as low as possible, the degrees of ϕ and ψ should be minimal. There is a tradeoff between the degrees of these two functions. If ψ is minimal (the identity), then ϕ must be at least cubic to have enough degrees of freedom to allow our surface to meet the boundary with a C^2 join. This situation will to lead to a binonic (bidegree 9) solution for $\mathcal{C}(l,u,v)$. We can do better if we minimize the bidegree of ϕ.

Our approach is to use the simplest possible (polynomial) ϕ and then to solve for a the function ψ that preserves second order contact with the boundary surface $\mathcal{B}$. We choose ϕ to be the bilinear function

$$\phi_x(u,v) = \mathbf{B}^1(u)\begin{bmatrix} 0 & C_n \\ 1 & 1 \end{bmatrix}(\mathbf{B}^1(v))^T,$$
$$\phi_y(u,v) = \mathbf{B}^1(u)\begin{bmatrix} 0 & S_n \\ 0 & T_n \end{bmatrix}(\mathbf{B}^1(v))^T,$$

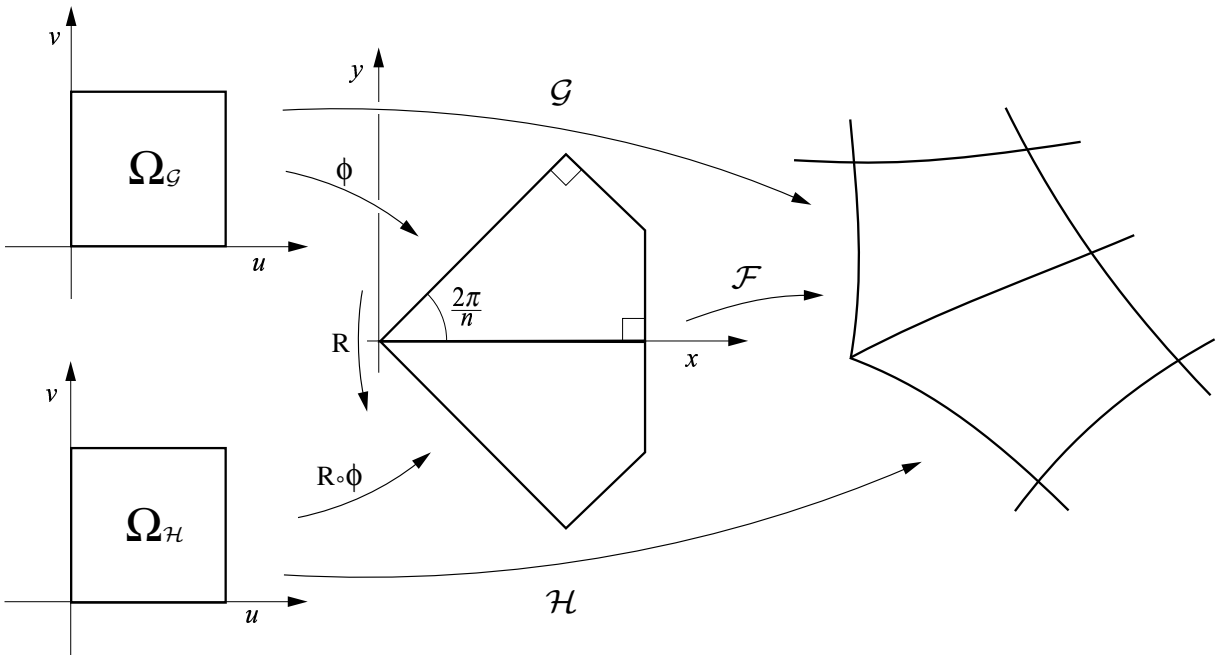

Figure 3: *We illustrate the mapping used in our definition of second order contact.*

where $C_n = \cos\frac{2\pi}{n}$, $S_n = \sin\frac{2\pi}{n}$, and $T_n = \tan\frac{\pi}{n}$. The geometry of ϕ is illustrated in Figure 3.

We can now expand $\mathbf{G}^1$ and $\mathbf{G}^2$ using ϕ and patches $\mathcal{G}$ and $\mathcal{H}$ of any degree. The derivatives of these surfaces at the endpoints $(1,0)$ and $(0,1)$ will be determined from the boundary surface $\mathcal{B}$. This will give us a collection of known, and unknown, derivatives for $\mathcal{G}$ and $\mathcal{H}$ in $\mathbf{G}^1$ and $\mathbf{G}^2$. We could proceed in the spatial domain to build an $\mathrm{O}(n)$ system of linear equations. The resulting system would be block circulant, and block diagonalized using the DFT. Each block would represent an $\mathrm{O}(1)$ linear system. These blocks would come in complex conjugate pairs, corresponding to the various frequencies decomposed by the DFT. Alternatively, we could formulate our constraint system directly in the frequency domain and consider the geometric object being constructed. Either approach is valid, but we chose the later as a more direct approach.

7. Mode Patches

We now construct a single patch $\hat{\mathcal{C}}(l,u,v)$ in each frequency mode l that satisfies the second order smoothness conditions $\mathbf{G}^1$ and $\mathbf{G}^2$, while maintaining second order contact with corresponding boundary surface $\hat{\mathcal{B}}(l,u,v)$. We refer to the surfaces $\hat{\mathcal{C}}(l,u,v)$, $l = 0 \ldots n-1$ as *mode patches* to underscore their geometric significance in solving the problem at hand.

In the spatial domain, the Bézier form of surface $\mathcal{C}(k,u,v)$ will be piecewise polynomial, where the index k refers to individual tensor product patches ordered in a cyclic fashion about an extraordinary vertex. In the frequency domain, the surface $\hat{\mathcal{C}}(l,u,v)$ is a single complex vector valued polynomial; the index l refers to a distinct frequency band, or mode. Surface patches adjacent to $\hat{\mathcal{C}}(l,u,v)$ are found by a complex rotation. That is, by multiplication with E_n^l (clockwise), or $\bar{E}_n^l$ (counter-clockwise).

The importance of mode patches is that they are a geometric entity resulting from the diagonalizing nature of the DFT. They are not unlike the geometrically significant *eigen surfaces* from subdivision surface theory. The DFT transforms a problem involving $\mathrm{O}(n)$ constraints in the spatial domain to n problem instances involving $\mathrm{O}(1)$ constraints in each frequency mode. Each of these problem instances can be interpreted geometrically as solving for a single tensor product mode patch.

In Section 5 we formulated conditions that a pair of surface patches $\mathcal{G}$ and $\mathcal{H}$ must satisfy for the join along their common boundary $\mathcal{G}(u,0) = \mathcal{H}(u,0)$ to be G^2. We called these conditions *symmetric* due the presumed reflective symmetry of ϕ. In addition to this reflective symmetry, the ϕ we chose in the last section has rotational symmetry.

We will leverage the results of Section 5 by making the

assignments

$$\mathcal{G}(u,v) \leftarrow \hat{\mathcal{C}}(l,u,v),$$
$$\mathcal{H}(v,u) \leftarrow \bar{E}_n^l \hat{\mathcal{C}}(l,u,v),$$

and then expanding $\mathbf{G}^1$ and $\mathbf{G}^2$. Note that these smoothness conditions are now between the derivatives of $\hat{\mathcal{C}}(l,u,v)$ and a rotated copy of itself $E_n^l \hat{\mathcal{C}}(l,u,v)$

For reasons to be explained shortly, we parameterize $\hat{\mathcal{C}}(l,u,v)$ as a biseptic polynomial and represent its Bézier coefficients as a complex vector valued 7-ring $\hat{\mathbf{c}}_{ij}^l$. We form the products involving ϕ and derivatives of $\hat{\mathcal{C}}(l,u,v)$ according to $\mathbf{G}^1$ and $\mathbf{G}^2$ to get polynomials of degree 7 and 8, respectively. We represent the Bézier coefficients of these polynomials as $\mathbf{g}^1$ and $\mathbf{g}^2$; we list these in Appendix A. The second order smoothness constraints on mode patch $\hat{\mathcal{C}}(l,u,v)$ correspond to these coefficients vanishing.

Two of the constraints, corresponding to $\mathbf{g}_7^1$ and $\mathbf{g}_8^2$, are automatically satisfied by our choice of ϕ. We can satisfy four more constraints $\mathbf{g}_5^1$, $\mathbf{g}_6^1$, $\mathbf{g}_6^2$ and $\mathbf{g}_7^2$ by finding a reparameterization ψ that modifies the derivatives along the two external boundaries ($u=1$, $v=1$) while preserving second order contact with the boundary surface $\mathcal{B}$.

8. Boundary Reparameterization

We now construct a reparameterization

$$\mathcal{C} = \mathcal{B} \circ \psi,$$

where $\psi\colon \mathbb{R}^2 \to \mathbb{R}^2$ so that $\mathcal{C}$ and $\mathcal{B}$ will have second order contact along the boundary edges $u=1$ and $v=1$. We find ψ subject to the four smoothness constraints $\mathbf{g}_5^1$, $\mathbf{g}_6^1$, $\mathbf{g}_6^2$ and $\mathbf{g}_7^2$.

At the outset we want ψ to be the identity along the edges of the unit square; and to be diagonally symmetric, that is $\psi(u,v) = \psi(v,u)$. Due to this symmetry, we need only consider one of the edges, we choose $v=1$. We assume in the following that functions are evaluated on $(u,1)$. From Definition 1 we see that

$$\overbrace{\hat{\mathcal{C}}^v}^{5} = \overbrace{\psi_x^v}^{3}\overbrace{\hat{\mathcal{B}}^x}^{2} + \overbrace{\psi_y^v}^{2}\overbrace{\hat{\mathcal{B}}^y}^{3}, \tag{5}$$

$$\overbrace{\hat{\mathcal{C}}^{vv}}^{7} = \overbrace{\psi_x^{vv}}^{5}\overbrace{\hat{\mathcal{B}}^x}^{2} + \overbrace{\psi_y^{vv}}^{4}\overbrace{\hat{\mathcal{B}}^y}^{3} + \overbrace{(\psi_x^v)^2}^{6}\overbrace{\hat{\mathcal{B}}^{xx}}^{1} + 2\overbrace{\psi_x^v\psi_y^v}^{5}\overbrace{\hat{\mathcal{B}}^{xy}}^{2} + \overbrace{(\psi_y^v)^2}^{4}\overbrace{\hat{\mathcal{B}}^{yy}}^{3}, \tag{6}$$

where we have placed the degree of each polynomial above it. We substitute (5) and (6)into $\mathbf{g}_5^1$, $\mathbf{g}_6^1$, $\mathbf{g}_6^2$ and $\mathbf{g}_7^2$ and find that the smoothness constraints can be solved (put to zero) if ψ_x^v and ψ_y^v are at least cubic and quadratic respectively. This implies by degree counting that each $\hat{\mathcal{C}}(l,u,v)$ must be bidegree 7. The polynomial degrees placed above terms in Equations (5) and (6) are intended as an aid in making this degree counting argument.

The degree restrictions on ψ_x^v and ψ_y^v, together with the identity and symmetry constraints, and by requiring that $\mathbf{g}_5^1$, $\mathbf{g}_6^1$, $\mathbf{g}_6^2$, and $\mathbf{g}_7^2$ vanish, determines ψ up to two degrees of freedom. We remove this freedom by minimizing the bidegree of ψ. This gives us ψ_x as the degree 4×3 tensor product $\psi_x(u,v) = \mathbf{B}^4(u)\,\Psi\,(\mathbf{B}^3(v))^T$, where

$$\Psi = \begin{bmatrix} 0 & 0 & 0 & 0 \\ \frac{1}{4} & \frac{5C_n^3-3C_n^2-15C_n+18}{12(C_n-2)(2C_n-3)} & \frac{C_n^2+2C_n-6}{12(C_n-2)} & \frac{1}{4} \\ \frac{1}{2} & \frac{C_n+3}{6} & \frac{C_n^2+3C_n-9}{9(C_n-2)} & \frac{1}{2} \\ \frac{3}{4} & \frac{C_n+9}{12} & \frac{C_n+9}{12} & \frac{3}{4} \\ 1 & 1 & 1 & 1 \end{bmatrix}.$$

Note that the symmetric ψ_y is degree 3×4, so we illustrate ψ for various values of n in Figure 4 as a bidegree 4 tensor product.

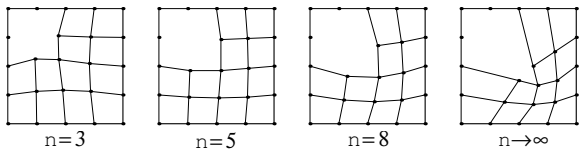

Figure 4: *The boundary edge reparameterization function ψ for various values of n. This missing control point does not come into play in our construction and has been omitted.*

Once the boundary derivatives of $\hat{\mathcal{C}}(l,u,v)$ have been determined from Equations (5) and (6), we are able to compute three layers of Bézier control points along the external boundary. We find $\hat{\mathbf{c}}_{7i}^l$ by degree elevation of $\hat{\mathbf{b}}_{3i}^l$. If $\hat{\mathbf{c}}_i^v$ and $\hat{\mathbf{c}}_i^{vv}$, are the Bézier coefficients of (degree raised) $\hat{\mathcal{C}}^v$ and $\hat{\mathcal{C}}^{vv}$ respectively, we have

$$\hat{\mathbf{c}}_{6i}^l = \hat{\mathbf{c}}_{7i}^l - \tfrac{1}{7}\hat{\mathbf{c}}_i^v, \tag{7}$$

$$\hat{\mathbf{c}}_{5i}^l = \hat{\mathbf{c}}_{7i}^l - \tfrac{12}{42}\hat{\mathbf{c}}_i^v + \tfrac{1}{42}\hat{\mathbf{c}}_i^{vv}, \tag{8}$$

$$\tag{9}$$

where $i = 0,\ldots,7$. Symmetric expressions hold for $\hat{\mathbf{c}}_{i6}^l$ and $\hat{\mathbf{c}}_{i5}^l$. These points are shown connected by lines in Figure 5.

Next, we solve the linear systems implied by the unsatisfied constraints among $\mathbf{g}^1$ and $\mathbf{g}^2$.

9. Internal Join

In the previous section we constructed a subset of the control points of the mode patches $\hat{\mathcal{C}}(l,u,v)$, by reparameterizing $\hat{\mathcal{B}}(l,u,v)$ along the external boundary corresponding to $u=1$ and $v=1$. Next, we consider the linear systems that must be solved to find the remaining control points among

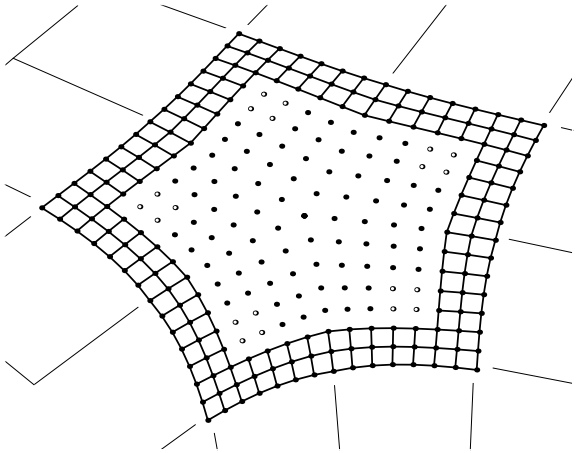

Figure 5: *The Bézier control points of the constructed biseptic patches. The points connected by lines on the interior come from boundary derivative reparameterization. The free floating points are found by solving the linear systems. The remaining hollow dots are found using a simple averaging procedure, see the text*

.

$\hat{\mathbf{c}}^l_{ij}$. Note that since mode patches $\hat{\mathcal{C}}(l,u,v)$ come in complex conjugate pairs, only $\lceil \frac{n}{2} \rceil$ systems need to be solved.

There are 11 remaining constraints from $\mathbf{g}^1$ and $\mathbf{g}^2$. The 15 points involved in $\mathbf{g}^1$ and $\mathbf{g}^2$ that we have found thus far are shown to the right of line in following diagram

$$\begin{array}{ccccc|ccc} & & \hat{\mathbf{c}}_{22} & \hat{\mathbf{c}}_{32} & \hat{\mathbf{c}}_{42} & \hat{\mathbf{c}}_{52} & \hat{\mathbf{c}}_{62} & \hat{\mathbf{c}}_{72} \\ & \hat{\mathbf{c}}_{11} & \hat{\mathbf{c}}_{21} & \hat{\mathbf{c}}_{31} & \hat{\mathbf{c}}_{41} & \hat{\mathbf{c}}_{51} & \hat{\mathbf{c}}_{61} & \hat{\mathbf{c}}_{71} \\ \hat{\mathbf{c}}_{00} & \hat{\mathbf{c}}_{10} & \hat{\mathbf{c}}_{20} & \hat{\mathbf{c}}_{30} & \hat{\mathbf{c}}_{40} & \hat{\mathbf{c}}_{50} & \hat{\mathbf{c}}_{60} & \hat{\mathbf{c}}_{70} \\ & & \hat{\mathbf{c}}_{12} & \hat{\mathbf{c}}_{13} & \hat{\mathbf{c}}_{14} & \hat{\mathbf{c}}_{15} & \hat{\mathbf{c}}_{16} & \hat{\mathbf{c}}_{17} \\ & & & \hat{\mathbf{c}}_{23} & \hat{\mathbf{c}}_{24} & \hat{\mathbf{c}}_{25} & \hat{\mathbf{c}}_{26} & \hat{\mathbf{c}}_{27} \end{array}$$

and the 17 unknown points are shown to the left. We must now solve linear systems involving 11 equations in 17 unknowns. Since the systems are under determined, we have degrees of freedom that must be removed. Our current approach to removing this freedom is to introduce additional constraints.

We constrain the degree of boundary curves. In general, the internal boundaries curves can be as high as degree 7. However, we constrain these curves to be cubic when $l = 0, 1$, quartic when $l = 2$, and quintic when $l > 2$. In addition to the boundary curve, we constrain the degree of the functions relating to transversal derivatives. Let $\mathbf{h}^0$, $\mathbf{h}^1$, and $\mathbf{h}^2$ be the power basis coefficients of the degree 7 polynomials $\mathcal{G}$, $\mathcal{G}^v - \mathcal{H}^v$, and $\mathcal{G}^{vv} + \mathcal{H}^{vv}$, respectively (where $\mathcal{G}(u,v) \leftarrow \hat{\mathcal{C}}(l,u,v)$, and $\mathcal{H}(v,u) \leftarrow \bar{E}^l_n \hat{\mathcal{C}}(l,v,u)$).

Precisely which set of constraints are needed to form independent sets will depend on l. All systems need the following 14 constraints to vanish

$$\mathbf{g}^1_i, \mathbf{g}^2_{i+1}, i = 0, \ldots, 4, \quad \text{and} \quad \mathbf{h}^0_6, \mathbf{h}^0_7, \mathbf{h}^2_6, \mathbf{h}^2_7.$$

We also require the following to vanish, depending on l

$$\begin{array}{llll} l = 0 & \mathbf{h}^0_4 & \mathbf{h}^0_5 & \mathbf{h}^2_5 \\ l = 1 & \mathbf{g}^2_0 & \mathbf{h}^0_5 & \mathbf{h}^2_5 \\ l = 2 & \mathbf{h}^0_5 & \mathbf{h}^1_7 & \hat{\mathbf{c}}_{00} \\ l > 2 & \mathbf{h}^1_7 & \hat{\mathbf{c}}_{10} & \hat{\mathbf{c}}_{20} \end{array}$$

For each $l = 0, \ldots, \lfloor \frac{n}{2} \rfloor$, we now have a 17×17 system that can be solved analytically with symbolic algebra software. Note that the matrix associated with each system depends only on valence n and frequency mode l, and not on the control mesh. There are three (known) exceptions to the constraint formation rules just given. These correspond to $n = 3$ with $l = 0, 1$, and $n = 6$ with $l = 3$. In these cases, we modify the constraint sets slightly. The control points found as solutions to the linear systems are shown (in the spatial domain) as isolated solid dots in figure 5.

We still have 4 unknown control points $\hat{\mathbf{c}}_{33}$, $\hat{\mathbf{c}}_{43}$, $\hat{\mathbf{c}}_{34}$, and $\hat{\mathbf{c}}_{44}$ at the center of each patch. We find positions for these points by minimizing the degrees of the curves represented by $\hat{\mathbf{c}}_{3i}$, $\hat{\mathbf{c}}_{4i}$, $\hat{\mathbf{c}}_{i3}$, and $\hat{\mathbf{c}}_{i4}$, $i = 0, \ldots, 7$, and averaging the result. These are shown as hollow dots in figure 5.

The points found in this section complete the biseptic mode patches $\hat{\mathcal{C}}(l,u,v)$. We transform the mode patches $\hat{\mathcal{C}}(l,u,v)$ back to the spatial domain to obtain the final G^2 surface $\mathcal{C}(k,u,v)$, as illustrated in Figure 5. Recovering the basis functions $\mathbf{A}(k,u,v)$ needed to form the surface $\mathcal{A}(k,u,v)$ (see Equation 1) is a straightforward linear algebra exercise.

10. Results

We illustrate our construction on a few control meshes in Figure 6.

11. Discussion

The issue of curvature continuity for subdivision surfaces will likely stimulate considerable research in the coming years. Subdivision algorithms in general, and the Catmull & Clark algorithm in particular, are popular because 1) their ability to model surfaces of arbitrary topological type, and 2) their simplicity of specification and implementation. Ideally, in addition to producing fair shapes, one would like a curvature continuous free form surface that is also simple to specify and implement.

One possibility would be a new subdivision algorithm. However, Prautzsch [Pra98] uses a degree argument to show that no modification to the spectrum of the subdivision matrix can generate G^2 surfaces. This leaves non-stationary schemes, where the subdivision masks do not stay constant. For such a scheme to be G^2 it must reproduce quadratic polynomials. However, for the surface to be fair the masks must

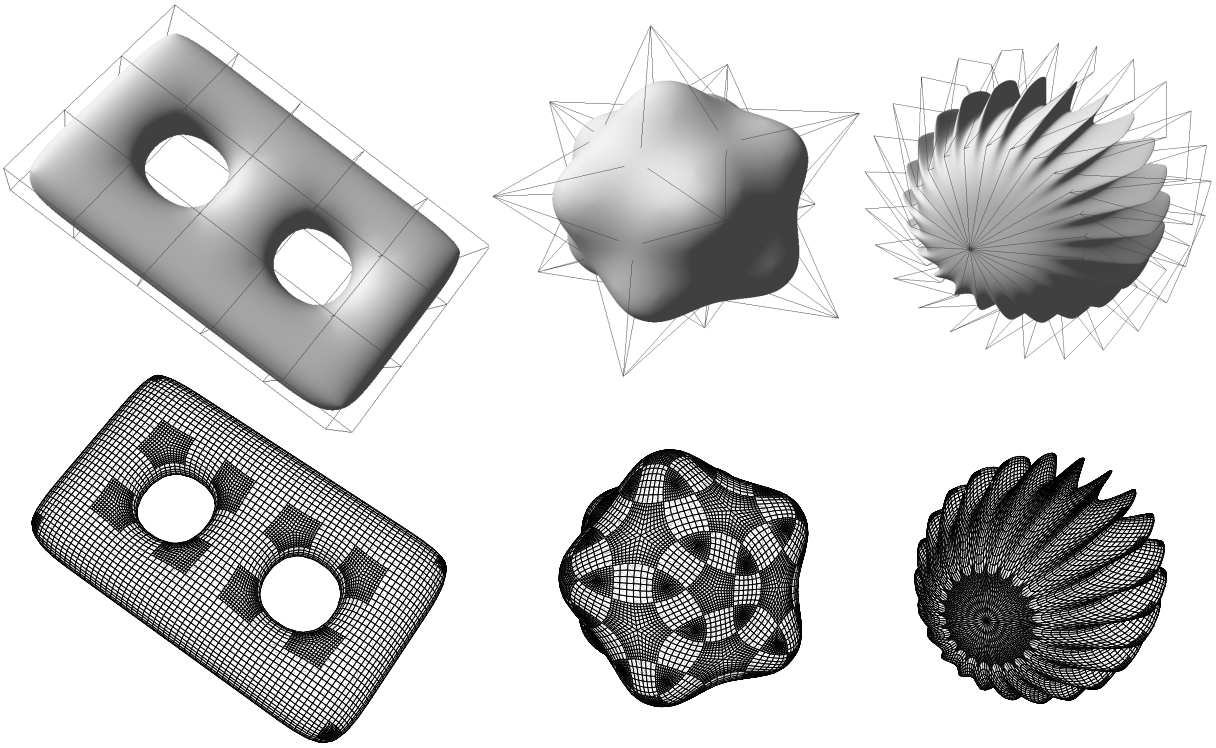

Figure 6: *Our construction applied to three control meshes. The top row shows the control mesh and resulting surfaces. The bottom row illustrates the corresponding bicubic and biseptic patches.*

also dampen high frequencies present in the control mesh. To date, these challenges remain open, and it is unclear if the resulting algorithm(s) will possess the simplicity of popular stationary subdivision schemes. Even so, subdivision will never remove topologically singular extraordinary vertices, it will only shrink them. This motivates alternatives to recursive refinement and smoothing.

Parametric surfaces are one such alternative. A framework is needed to compare the merits of various G^2 parametric surface schemes. From a strictly quantitative standpoint, the issues to consider are the number of subdivision steps needed, the number of patches required to fill the hole, and the polynomial bidegree of the solution. The most closely related previous schemes [Pra97, GZ99, Pet02] assume extraordinary vertex isolation consistent with at least a 2-ring. In order to fill the hole without modifying the boundary data using any of these schemes, at least $4n$ patches are needed. While the bi-degree of tensor product patches produced are less than the 7×7 patches presented here, many more control points in total must be computed. The tradeoff becomes one of patch count versus polynomial bidegree. We suggest that slightly lower degree may not be an advantage if $4\times$ as many surface patches must be computed, stored and processed. While each lower degree patch may have less cost, one must consider entire system throughput as a deciding factor.

From a qualitative standpoint, fairness of the resulting shapes is the important metric. Unfortunately, this is a subjective notion that may depend on the shape and connectivity of the control mesh. We have generated surfaces from a wide variety of control meshes using our scheme and found the surfaces to behave much like the corresponding Catmull & Clark surface. A more rigorous side by side comparison of available methods is needed.

It is important to point out that the shapes generated by strictly adhering to the procedure outlined in this paper may not be as fair as is possible, given the available degrees of freedom in our construction. In Section 9, we needed to remove degrees of freedom in under determined linear systems. Our approach of adding additional constraints resulted in unique solutions to these systems, but is admittedly ad-hoc.

Constraining the positions of $\hat{\mathbf{c}}_{00}$, $\hat{\mathbf{c}}_{10}$, and $\hat{\mathbf{c}}_{20}$, ensures that mode patches have the property that only $\hat{\mathcal{C}}(0,u,v), \hat{\mathcal{C}}(1,u,v)$, and $\hat{\mathcal{C}}(2,u,v)$ contribute to the second order behavior at the shared corner point $\mathcal{C}(k,0,0)$. Only $\hat{\mathcal{C}}(0,u,v)$ contributes to the position and $\hat{\mathcal{C}}(1,u,v)$ to the tangent plane of $\mathcal{C}(k,0,0)$. All other higher order mode patches

$\hat{\mathcal{C}}(l,u,v), l \geq 3$, are 'flat', having zero curvature at $(0,0)$. Note that only the higher order $l \geq 3$ mode patches are flat at $(0,0)$, not the resulting spatial domain surface.

Other methods of finding surfaces in our solution space are certainly possibly. This might include *better* affine combination, that yield *better* shapes. Or, a non-linear optimization procedure could be used to find the shape that minimizes some energy functional. Ideally, we would like to express the Bézier control points of the hole filling surfaces, in either the spatial or frequency domains, as simple affine combinations of an extraordinary vertex 2-ring.

From a modeling systems perspective, our approach is straightforward. We represent the initial control mesh as an edge based graph that represents the primal (vertices) and dual (faces). The surface is completely defined by a collection of 2-rings that are in one-to-one correspondence with the vertices, faces, and edges of this graph. For 2-rings associated with edges, valence is always 4 resulting in bicubic patches. The patches may be processed independently, or as a 2-ring depending on what part of the graphics pipeline they are in. Adaptive rendering might take place on a per patch basis, while transforms and vertex processing could happen on 2-rings. Each bicubic patch is encoded by $4 \times 4 = 16$ vertices; each biseptic patch is encoded by $8 \times 8 = 64$ vertices.

The advantage of our approach is the built in compatibility with the now standard Catmull & Clark modeling paradigm. At least two steps of Catmull & Clark subdivision must be performed. The first step of Catmull & Clark turns an arbitrary 2-manifold control mesh into a quad mesh. The second step guarantees that all extraordinary vertices are surrounded by 2-rings. More steps could be performed locally or globally to get arbitrarily close to the corresponding Catmull & Clark limit surface.

Using the mode patch construction technique, we are able to significantly reduce the cost of dealing with high valence vertices. For a general valence n vertex, we need to find n mode patches (counting each complex component). We can considerably reduce this number by effectively *low pass filtering* the DFT of a 2-ring control net. That is, if we truncate all frequencies beyond, say $l = 2$, we do not need to compute the corresponding mode patches since their coefficients will be zero. This is a reasonable proposition when one considers that this is related to what happens in a subdivision step. The highest frequency terms are shrinking the fastest, as a low pass filter. By applying such a filter, the cost of storing and processing a high valence vertex is reduced from $O(n)$ to $O(1)$. We need only store a mode patch for each surviving frequency. The n spatial domain patches are instantiated, then rendered. Such a low pass filter will affect the positions of 2-ring control points; this is, the boundary data will be modified. Filtering should happen on a mesh that has been subdivided at least 3 times to ensure proper 2-ring isolation.

12. Conclusions

We have demonstrated that n-valent extraordinary vertex holes, present in Catmull & Clark subdivision surfaces can be filled, to second order contact, with n bidegree 7 tensor product patches. Our approach has been to solve the problem in the frequency domain where we fill the hole in each spectral band with a single tensor product patch we call a mode patch. Combining these mode patches back in the spatial domain leads to second order continuity over extraordinary vertices.

Our construction has involved transformations between the spatial and frequency domains, and the analytic solutions to multiple 17×17 systems. While these steps have been used to derive our solution, they are not strictly necessary parts of an implementation. Ultimately, the control points of the biseptic patches in the spatial domain are found as affine combinations of the corresponding spatial domain 2-ring. It should be possible to derive these affine combinations, or masks, explicitly.

We have not resolved the important issue of the convex hull property. That is, is there a solution for the control points of the biseptic patches $\mathcal{C}(k,u,v)$ that are strictly convex combinations of the 2-ring points $\mathbf{a}$? Explicitly computing the various masks for the Bézier control points $\mathbf{c}^k$ will result in corresponding trigonometric functions parameterized by valence n. If the functions are entirely positive, then the convex hull property would be realized. If these functions are not entirely positive, it might be possible to arrange for settings of the degrees of freedom found in our construction that do lead to positive functions. These issues are left for future work.

We have not considered surfaces with boundary. In this extension, the surface should interpolate the cubic B-spline defined by the boundary edges (as is done with Catmull & Clark surfaces). Also, the modeling of sharp creases and other surface features should be included in this framework, we leave this to future work as well.

References

[BH95] BRIGGS W., HENSON V.: *The DFT*. SIAM, 1995.

[CC78] CATMULL E., CLARK J.: Recursively generated B-spline surfaces on arbitrary topological meshes. *Computer Aided Design 10*, 6 (1978), 350–355.

[DeR85] DEROSE A.: *Geometric Continuity: A Parametrization Independent Measure of Continuity for Computer Aided Geometric Design*. PhD thesis, Berkeley, 1985. also tech report UCB/CSD 86/255.

[DKT98] DEROSE T., KASS M., TRUONG T.: Sudivision surfaces in character animation. In *Siggraph 1998, Computer Graphics Proceedings* (1998), pp. 85–94.

[DS78] DOO D., SABIN M.: Behaviour of recursive division surfaces near extraordinary points. *Computer Aided Design 10*, 6 (1978), 356–360.

[Far01] FARIN G.: *Curves and Surface for CAGD: A Practical Guide*. Morgan-Kaufmann, 2001.

[GH89] GREGORY J., HAHN J.: A C^2 polygonal surface patch. *Computer Aided Geometric Design 6*, 1 (1989), 69–76.

[GZ99] GREGORY J., ZHOU J.: Irregular C^2 surface construction using b-polynomial rectangular patches. *Computer Aided Geometric Design 16*, 5 (1999), 423–435.

[Nee97] NEEDHAM T.: *Visual Complex Analysis*. Oxford University Press, 1997.

[Pet96] PETERS J.: Curvature continuous spline surfaces over irregular meshes. *Computer Aided Geometric Design 13*, 2 (1996), 101–131.

[Pet02] PETERS J.: C^2 free-form surfaces of degree (3,5). *Computer Aided Geometric Design 19*, 2 (2002), 113–126.

[Pet03] PETERS J.: Smoothness, fairness and the need for better multi-sided patches. In *Topics in algebraic geometry and geometric modeling* (2003), vol. 334.

[Pra97] PRAUTZSCH H.: Freeform splines. *Computer Aided Geometric Design 14*, 3 (1997), 201–206.

[Pra98] PRAUTZSCH H.: Smoothness of subdivision surfaces at extraordinary points. *Advances in Computational Mathematics 9* (1998), 377–390.

[PU00] PRAUTZSCH H., UMLAUF G.: Triangular G^2 splines. In *Curves and Surfaces in Design, Saint-Malo 99*, Laurent P., Sablonniére P.,, Schumaker L., (Eds.). Vanderbilt University Press, 2000, pp. 335–342.

[Rei95] REIF U.: A unfied approach to subdivision algorithms near extraordinary vertices. *Computer Aided Geometric Design 12* (1995), 153–174.

Appendix A: Appendix

We expand the second order smoothness constraints $\mathbf{G}^1$ and $\mathbf{G}^2$ with $\hat{\mathcal{C}}(l,u,v)$ as a bidegree 7 tensor product and using ϕ defined in Section 6. We simplify our notation in the following by making the assignments $C \leftarrow C_n, S \leftarrow S_n, T \leftarrow T_n, E \leftarrow E^j$, and $\mathbf{c} \leftarrow \hat{\mathbf{c}}$

$\mathbf{G}^1$

$$\mathbf{g}_0^1 = (C-1)\,\mathbf{c}_0 + (C^j - C)\,\mathbf{c}_{10}$$

$$\mathbf{g}_1^1 = 2\,(6C-7)\,\mathbf{c}_{10} + 7\,(1+\bar{E})\,\mathbf{c}_{11} - 12C\,\mathbf{c}_{20}$$

$$\mathbf{g}_2^1 = 7\bar{E}\,\mathbf{c}_{12} + 2\,(5C-7)\,\mathbf{c}_{20} + 7\,\mathbf{c}_{21} - 10C\,\mathbf{c}_{30}$$

$$\mathbf{g}_3^1 = 7\bar{E}\,\mathbf{c}_{13} + 2\,(4C-7)\,\mathbf{c}_{30} + 7\,\mathbf{c}_{31} - 8C\,\mathbf{c}_{40}$$

$$\mathbf{g}_4^1 = 7\bar{E}\,\mathbf{c}_{14} + 2\,(3C-7)\,\mathbf{c}_{40} + 7\,\mathbf{c}_{41} - 6C\,\mathbf{c}_{50}$$

$$\mathbf{g}_5^1 = 7\bar{E}\,\mathbf{c}_{15} + 2\,(2C-7)\,\mathbf{c}_{50} + 7\,\mathbf{c}_{51} - 4C\,\mathbf{c}_{60}$$

$$\mathbf{g}_6^1 = 7\bar{E}\,\mathbf{c}_{16} + 2\,(C-7)\,\mathbf{c}_{60} + 7\,\mathbf{c}_{61} - 2C\,\mathbf{c}_{70}$$

$$\mathbf{g}_7^1 = \bar{E}\,\mathbf{c}_{17} - 2\,\mathbf{c}_{70} + \mathbf{c}_{71}$$

$\mathbf{G}^2$

$$\mathbf{g}_0^2 = 98CS(\bar{E}-1)\,\mathbf{c}_{11} + 28\,\mathbb{I}S^j\,((6\,(C-1)\,S + CT)\,\mathbf{c}_{10} + 3S\mathbf{c}_{20})$$

$$\begin{aligned}\mathbf{g}_1^2 = {} & 2\,\mathbb{I}TS^j\,((7C-6)\,\mathbf{c}_{10} + 3\,\mathbf{c}_{20}) - 7S((5C-6)\,(\bar{E}-1)\,\mathbf{c}_{11} \\ & - 3\,(1+2C\bar{E})\,\mathbf{c}_{12} + 3\,(2C+\bar{E})\,\mathbf{c}_{21})\end{aligned}$$

$$\begin{aligned}\mathbf{g}_2^2 = {} & 2\,(1-C)\,T\,(\bar{E}-1)\,\mathbf{c}_{11} + (T + ((6-4C)\,S + CT)\,\bar{E})\,\mathbf{c}_{12} + 5CS\bar{E}\,\mathbf{c}_{13} \\ & + ((4C-6)\,S - CT - T\bar{E})\,\mathbf{c}_{21} - 3S(\bar{E}-1)\,\mathbf{c}_{22} - 5CS\,\mathbf{c}_{31}\end{aligned}$$

$$\begin{aligned}\mathbf{g}_3^2 = {} & 3\,(5C-6)\,T\,\mathbf{c}_{21} + 9\,T\,\mathbf{c}_{22} + \bar{E}\,(3\,(6-5C)\,T\,\mathbf{c}_{12} \\ & - 5\,(3\,(C-2)\,S - 2CT)\,\mathbf{c}_{13} + 20CS\,\mathbf{c}_{14} - 9\,T\,\mathbf{c}_{22} - 15S\,\mathbf{c}_{23}) \\ & - 10CT\,\mathbf{c}_{31} + 15S((C-2)\,\mathbf{c}_{31} + \mathbf{c}_{32}) - 20CS\,\mathbf{c}_{41}\end{aligned}$$

$$\begin{aligned}\mathbf{g}_4^2 = {} & \bar{E}\,((6-4C)\,T\,\mathbf{c}_{13} + (6S - 2CS + 3CT)\,\mathbf{c}_{14} + 3CS\,\mathbf{c}_{15} \\ & - 3\,T\,\mathbf{c}_{23} - 3S\,\mathbf{c}_{24}) + 2\,(2C-3)\,T\,\mathbf{c}_{31} + 2\,(C-3)\,S\,\mathbf{c}_{41} \\ & + 3S\,\mathbf{c}_{42} - 3\,(CT\,\mathbf{c}_{41} + CS\,\mathbf{c}_{51} - T\,\mathbf{c}_{32})\end{aligned}$$

$$\begin{aligned}\mathbf{g}_5^2 = {} & \bar{E}\,(5\,(C-2)\,T\,\mathbf{c}_{14} + ((C-6)\,S - 4CT)\,\mathbf{c}_{15} - 2CS\,\mathbf{c}_{16} \\ & + 5\,T\,\mathbf{c}_{24} + 3S\,\mathbf{c}_{25}) - 5\,(C-2)\,T\,\mathbf{c}_{41} - 5\,T\,\mathbf{c}_{42} \\ & - (C-6)\,S\,\mathbf{c}_{51} + 4CT\,\mathbf{c}_{51} - 3S\,\mathbf{c}_{52} + 2CS\,\mathbf{c}_{61}\end{aligned}$$

$$\begin{aligned}\mathbf{g}_6^2 = {} & \bar{E}\,(6\,(3-C)\,T\,\mathbf{c}_{15} + (6S + 5CT)\,\mathbf{c}_{16} + CS\,\mathbf{c}_{17} - 9\,T\,\mathbf{c}_{25} - 3S\,\mathbf{c}_{26}) \\ & + 6\,(C-3)\,T\,\mathbf{c}_{51} + 9\,T\,\mathbf{c}_{52} - 6S\,\mathbf{c}_{61} - 5CT\,\mathbf{c}_{61} + 3S\,\mathbf{c}_{62} - CS\,\mathbf{c}_{71}\end{aligned}$$

$$\begin{aligned}\mathbf{g}_7^2 = {} & \bar{E}\,(7\,(6-C)\,T\,\mathbf{c}_{16} + ((6+C)\,S + 6CT)\,\mathbf{c}_{17} - 3\,(7\,T\,\mathbf{c}_{26} + S\mathbf{c}_{27})) \\ & + 7\,(C-6)\,T\,\mathbf{c}_{61} - (6+C)\,S\,\mathbf{c}_{71} + 3\,T\,(7\,\mathbf{c}_{62} - 2C\,\mathbf{c}_{71}) + 3S\,\mathbf{c}_{72}\end{aligned}$$

$$\mathbf{g}_8^2 = \bar{E}\,(2\,\mathbf{c}_{17} - \mathbf{c}_{27}) - 2\,\mathbf{c}_{71} + \mathbf{c}_{72}$$